Solution AFM Studies of Human Swi-Snf and Its Interactions with MMTV DNA and Chromatin

H. Wang,* R. Bash,*† S. M. Lindsay,*†‡ and D. Lohr†

*Arizona Biodesign Institute, †Department of Chemistry and Biochemistry, and ‡Department of Physics and Astronomy, Arizona State University, Tempe, Arizona 85287

ABSTRACT   ATP-dependent nucleosome remodeling complexes are crucial for relieving nucleosome repression during transcription, DNA replication, recombination, and repair. Remodeling complexes can carry out a variety of reactions on chromatin substrates but precisely how they do so remains a topic of active inquiry. Here, a novel recognition atomic force microscopy (AFM) approach is used to characterize human Swi-Snf (hSwi-Snf) nucleosome remodeling complexes in solution. This information is then used to locate hSwi-Snf complexes bound to mouse mammary tumor virus promoter nucleosomal arrays, a natural target of hSwi-Snf action, in solution topographic AFM images of surface-tethered arrays. By comparing the same individual chromatin arrays before and after hSwi-Snf activation, remodeling events on these arrays can be monitored in relation to the complexes bound to them. Remodeling is observed to be: inherently heterogeneous; nonprocessive; able to occur near and far from bound complexes; often associated with nucleosome height decreases. These height decreases frequently occur near sites of DNA release from chromatin. hSwi-Snf is usually incorporated into nucleosomal arrays, with multiple DNA strands entering into it from various directions, + or − ATP; these DNA paths can change after hSwi-Snf activation. hSwi-Snf appears to interact with naked mouse mammary tumor virus DNA somewhat differently than with chromatin and ATP activation of surface-bound DNA/hSwi-Snf produces no changes detectable by AFM.

INTRODUCTION

ATP-dependent nucleosome remodeling complexes relieve the inherently repressive effects of nucleosome structure (1–9), thus enabling processes like transcription, replication, repair, and recombination throughout the genome (10–15). Many such complexes have been identified. They can carry out a variety of ''remodeling'' reactions: nucleosome sliding; *trans* octamer transfer; nucleosome dimer formation; and DNA dissociation from the nucleosome. Despite intensive study, uncertainties remain concerning precise mechanisms and, in some cases, the molecular nature of the changes being monitored.

In vitro studies of these complexes have typically relied on ensemble-average approaches that monitor changes in DNA accessibility (to nucleases or transcription factors) or changes in DNA supercoiling to follow remodeling activity. In the first single-molecule studies, using electron microscopy (EM) (16) or atomic force microscopy (AFM) (17) approaches, remodeling was assessed by comparing images of chromatin samples deposited before versus after the activation of remodeling by ATP addition; this involved comparing two distinct populations of molecules. Recently, we described an AFM approach that can image, in solution, the same individual molecules before and after ATP addition (hSwi-Snf activation). This approach provides direct information on the changes carried out by remodeling complexes on single molecules (18). Those studies used the human Swi-Snf

(hSwi-Snf) remodeling complex and nucleosomal arrays reconstituted on a physiologically relevant DNA template, the mouse mammary tumor virus-long terminal repeat (MMTV-LTR) promoter, a natural in vivo target of hSwi-Snf during MMTV gene activation (19–21).

To be able to compare the same individual molecules before and after ATP addition, MMTV nucleosomal arrays are preincubated with hSwi-Snf, deposited on a glutaraldehyde-aminopropyltriethoxysilane (GD-APTES) derivatized mica surface, which chemically tethers the arrays (via the histones), and imaged in a flow cell attached to the AFM (18). Significant changes are observed in 5–10% of the individual chromatin molecules after ATP addition; various controls demonstrated that these changes reflect remodeling activity. The changes vary both in nature and extent and often take place on molecules in close spatial proximity on the surface. That remodeling complexes can carry out a variety of alterations on a single chromatin substrate indicates that single molecule approaches will ultimately be needed to understand the actions of these important complexes. Most of the events observed involve changes in DNA path, either local or long range, within the arrays. The two most common changes, DNA release from nucleosomes and rewiring (significantly altering) of the DNA topology, were never observed in controls and thus are clearly hSwi-Snf (not technique) induced changes (18). In the previous work, we did not address the important questions of where the hSwi-Snf molecules were located in relation to the remodeling events and what specific chromatin alterations were involved in individual remodeling events.

In this work, we describe solution topographic and recognition AFM imaging studies of the hSwi-Snf complex itself.

This information is then used to identify hSwi-Snf complexes in topographic images of chromatin plus hSwi-Snf. This permits the analysis of hSwi-Snf interactions with chromatin and quantitative studies of specific remodeling events occurring on chromatin molecules containing the complex. The interactions of hSwi-Snf with naked MMTV DNA (no nucleosomes) and the effects of ATP activation on surface-bound DNA/hSwi-Snf were also analyzed for comparison to the chromatin results. All imaging was done in solution.

EXPERIMENTAL PROCEDURES

Chromatin/hSwiSnf

MMTV arrays were reconstituted to subsaturating levels (with HeLa histones, a generous gift of Dr. Jaya Yodh) and remodeling reactions using hSwi-Snf (a generous gift from Gordon Hager) were carried out as described previously (18,22). hSwi-Snf was purified by standard procedures, as described (18). Use of subsaturated arrays is required for AFM studies on this template, for several reasons (22). For the hSwi-Snf + MMTV DNA studies, molar ratios of 1:1, 1:2, 1:3, and 1:6 hSwi-Snf/DNA were analyzed. The DNA is an ~1.9 kb NcoI-SphI fragment that contains the MMTV promoter region (23), which has been used before for AFM studies of chromatin (18,22). For the hSwi-Snf + chromatin analyses, molar ratios of 1:6 hSwi-Snf/nucleosomal array (1 hSwi-Snf per 20–40 individual nucleosomes), 1:4.5 or 1:3 were used. The lower (1:6) ratio actually gave the clearest results in general and changes were as robust as when higher concentrations of hSwi-Snf were used. Thus, this molar ratio was used for most of the studies described here. The higher concentrations of hSwi-Snf also tend to increase the extent of aggregation of molecules into dense clumps in the chromatin+hSwi-Snf samples. The hSwi-Snf preparation contains bovine serum albumin (BSA) at a 4:1 molar ratio to hSwi-Snf. The BSA is necessary to maintain remodeling activity (18).

AFM imaging

The remodeling protocol has previously been described in detail (18). Briefly, samples (hSwi-Snf plus DNA or hSwi-Snf plus chromatin) were diluted and incubated in deposition buffer (10 mM NaCl/5 mM NaH$_2$PO$_4$, pH = 7.5) for 25 min, then deposited and imaged in the same buffer, before then after flowing 1 mM ATP (plus 1 mM Mg^{2+}) into the sample. The surface, GD-APTES, tethers nucleosomes (via the histones) but leaves the nucleosomal DNA as well as some histones relatively free to move (24). Imaging is done in solution in a flow cell linked to the AFM, as described (18). This arrangement allows ATP to be added, to activate hSwi-Snf, while still being able to scan the same individual molecules within the AFM image. The time between addition of ATP (after the completion of the first scan (−ATP)) and the start of the second scan (+ATP) was 30 min. Images were acquired in a scan time of 5 min per image. For imaging of hSwi-Snf alone, samples were either treated as described above or incubated with 1 mM ATP (plus 1 mM Mg^{2+}) then deposited.

For the analysis of chromatin remodeling occurring near hSwi-Snf complexes, 94 small areas showing significant chromatin changes (− versus + ATP) were selected from low-resolution images. Forty of these original 94 areas contained a hSwi-Snf (by the criteria used; see text) and a total of 64 complexes or ~1.5 per area. Eighteen of these were selected for detailed analysis, based on the clarity of the images, ability to follow the chromatin changes, etc.

Data analysis

Contour lengths and particle heights were measured using FemtoScan (Advanced Technologies Center, Moscow, Russia). Heights were taken as the peak heights relative to the local background. In all DNA distance measurements that involved nucleosomes, distances were measured from nucleosome centers and corrected for the extra 11 nm of histone core width when the path spans a nucleosome (5.5 nm when the nucleosome is at the end of the path).

AFM recognition imaging

E-type cantilever tips (Park Scientific, Santa Barbara, CA) for recognition imaging of hSwi-Snf samples were modified as described (25). Antibodies to hSwi-Snf (Upstate Scientific Biotechnology, Lake Placid, NY) were reacted with N-succinimidyl 3-(acetylthio)propionate (SATP, Sigma, St. Louis, MO) and purified on a PD-10 column (Amersham Pharmacia Biotech, Piscataway, NJ). The cantilevers were cleaned in an ultraviolet cleaner, vapor treated with APTES (24), and reacted with poly(ethylene glycol) (PEG) cross-linker (26) using triethylamine and CHCl$_3$. The SATP-labeled antibodies were then bound to the PEG cross-linkers with NH$_2$OH (Sigma) in buffer A (100 mM NaCl/ 50 mM NaH$_2$PO$_4$/1 mM EDTA, pH 7.5). The tips were then rinsed in PBS buffer and stored at 4°C until use. Imaging was done on a PicoPlus AFM with a Picotrec recognition imaging attachment (Molecular Imaging, Phoenix, AZ) with 6–8 nm amplitude oscillation at 9 kHz, imaging at 70% set point and scanning at 1 Hz.

The hSwi-Snf preparation used here contained BSA (necessary for remodeling activity (18)), in a molar ratio of 4:1 BSA/hSwi-Snf. No recognition is observed in samples of BSA at the concentrations present in hSwi-Snf and hSwi-Snf+chromatin samples when scanned with a BRG1 antibody-tethered tip. Therefore the BRG1 antibody does not recognize BSA. The recognition reaction of BRG1 antibody-tethered tips with hSwi-Snf is blocked when the BRG1 peptide used to generate the antibody is flowed into the cell, an important control demonstrating that the antibody recognition reaction of hSwi-Snf is specific (25). Unfortunately, the BRG1 antibodies (several from different sources were tried) were found to recognize nucleosomes very efficiently (>80%), a cross-reaction confirmed by standard ELISA assays (data not shown). Thus, BRG1 could not be used to identify hSwi-Snf in images containing chromatin.

RESULTS

Imaging the hSwi-Snf complex in solution

Samples of human Swi-Snf (hSwi-Snf) were deposited and imaged on GD-APTES mica, as in our previous chromatin studies (18,22). Particles of varying sizes are found in these images (Fig. 1 A); their heights were measured to characterize them. Height measurements are free of the '' tip-broadening'' artifacts that impact AFM width measurements but can be affected by imaging conditions. Those conditions were kept as constant as possible throughout these studies.

The heights of some representative complexes in Fig. 1 A are given in the figure legend and the distribution of heights obtained from analyses of a number of images like Fig. 1 A are shown in Fig. 2 A (open bars). Values range from ~7.5 to <1.5 nm, with two main classes, averaging ~3 and ~4.5 nm in height. hSwi-Snf incubated with ATP before deposition shows a similar distribution of particle heights (data not shown).

The hSwi-Snf sample contains BSA, which is required to maintain remodeling activity (18), and it is possible that the smaller particles could be BSA or BSA aggregates. To identify authentic hSwi-Snf complexes, we applied a recently
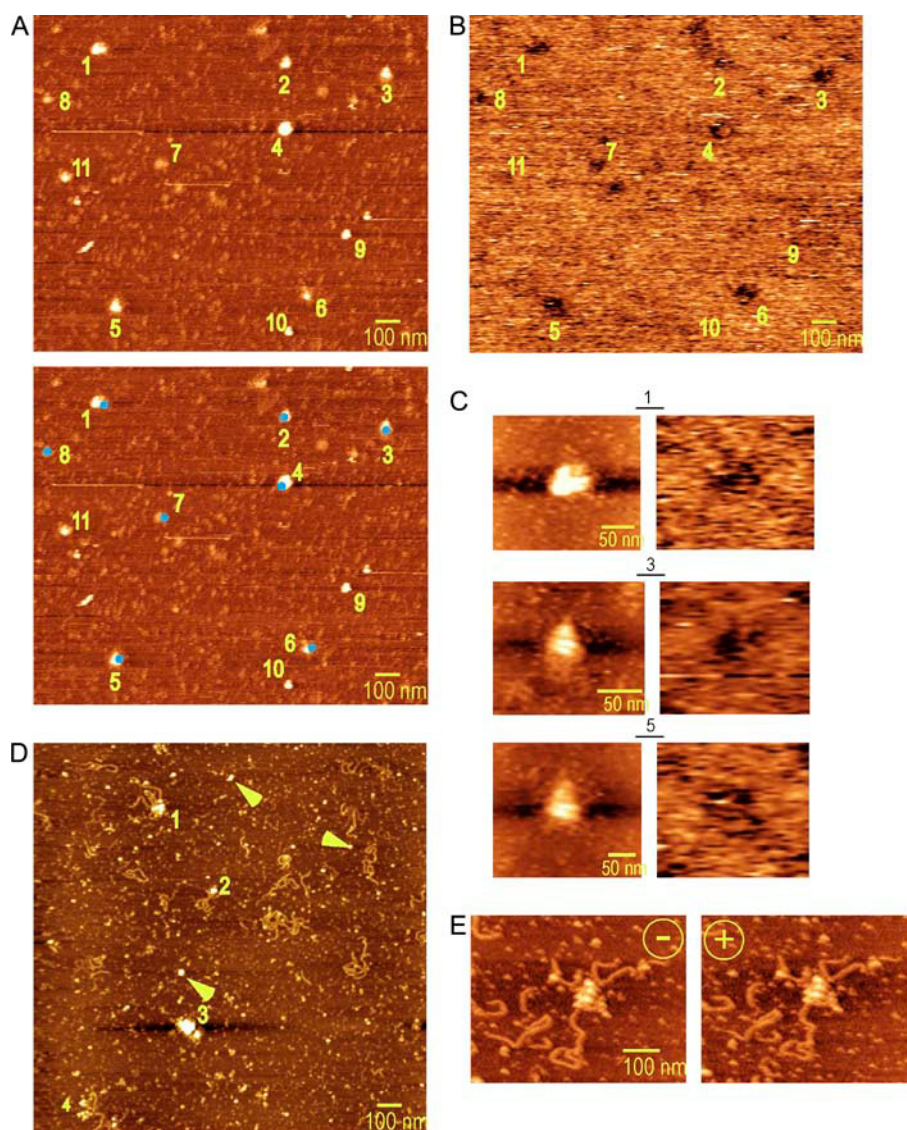
FIGURE 1 Images of hSwi-Snf and hSwi-Snf/DNA complexes. Topographic (*A*) and recognition (*B*) images of hSwi-Snf are shown. Some representative particles in images *A* and *B* are numbered. Particles 1–8 represent complexes in panel *A* that are recognized by the BRG1 antibody present on the tip during scanning (*B*). Their heights are: 1, 4.6 nm; 2, 3.7 nm; 3, 4.3 nm; 4, 6.0 nm; 5, 4.6 nm; 6, 3.0 nm; 7, 1.8 nm; 8, 2.2 nm. Particles 9–11 represent particles in panel *A* that are not (or only weakly) recognized by the BRG1 antibody during scanning. Their heights are: 9, 5.7 nm; 10, 4.2 nm; 11, 2.9 nm. Immediately below Fig 1 *A* is an image that superimposes recognition events for the numbered complexes in Fig. 1 *B* on the topographic image from Fig. 1 *A* (recognition events are identified by *blue dots*). Note that the sizes of particles in recognition images are often larger than in the corresponding topographic images. The blue dots are not meant to reflect recognition spot size, only the occurrence of strong recognition. The large size of recognition spots may reflect the effect of the antibody tether or other features (25). Higher-magnification topographic and recognition images of some complexes from panel *A* (*1*, *3*, and *5*) are compared side-by-side in panel *C*. Panel *D* shows an example of an image of hSwi-Snf plus DNA (1:1 molar ratio). Yellow arrows mark particles that are probably free hSwi-Snf complexes, i.e., not bound to DNA. The heights of the marked, DNA-bound complexes in panel *D* are: 1, 2.6 nm; 2, 2.3 nm; 3, 7.1 nm (with a 2.1-nm particle to the immediate lower right of the main particle); 4, 1.2 and 1.4 nm. Panel *E* shows an example of hSwi-Snf bound to DNA (1:6 hSwi-Snf/DNA molar ratio), imaged before (−) and after (+) ATP addition. The heights of the several (presumably) hSwi-Snf blobs in the center of the image are ~2 nm. The scale bars are 100 nm in images *A*, *B*, *D*, and *E* and 50 nm in image *C*.

developed technique called recognition imaging (25), which can identify specific types of molecules in AFM images. The technique uses an antibody-tethered AFM tip for scanning. It produces normal topographic images but whenever the antibody on the tip recognizes its antigen in the sample, the oscillating tip response is altered. The alteration can be converted into a ''recognition'' signal (see Experimental Procedures), which shows the locations of these antigen-antibody binding events, and thus the locations of a given type of molecule, in the image field. The recognition image is obtained simultaneously and is in exact spatial registration with the topographic image. Recognition has been shown to be specific and efficient (25).

To identify hSwi-Snf complexes, the deposited samples were scanned with tips containing an antibody against BRG1, a major catalytic ATPase subunit in these complexes (5,8,27). BRG1 antibodies specifically recognize the hSwi-Snf complex (see Experimental Procedures). The recognition image corresponding to the topographic image in Fig. 1 *A* shows that particles of all heights down to the shortest, <2 nm, can be recognized by the antibody (*dark spots*, Fig. 1 *B*). A composite image consisting of recognition events (identified by *blue dots* for complexes 1–8 in Fig. 1 *B*) superimposed on the topographic image from Fig. 1 *A* is shown immediately below Fig. 1 *A*. The height distribution of recognized particles for the entire data set confirms that particles of all heights can contain BRG1 (Fig. 2 *A*, *solid bars*). Thus BRG1, the catalytic core subunit of hSwi-Snf, can be found in various-sized complexes. Whether this variety of sizes is due to dissociation under these solution conditions or stoichiometric imbalances among the subunits (arising perhaps during cellular expression of the complex) or both is unknown. Recognition imaging was not applied to all topographic images; thus, the larger number of open versus solid bars in Fig. 2 *A* does not reflect a major lack of recognition. The average efficiency of BRG1 recognition for
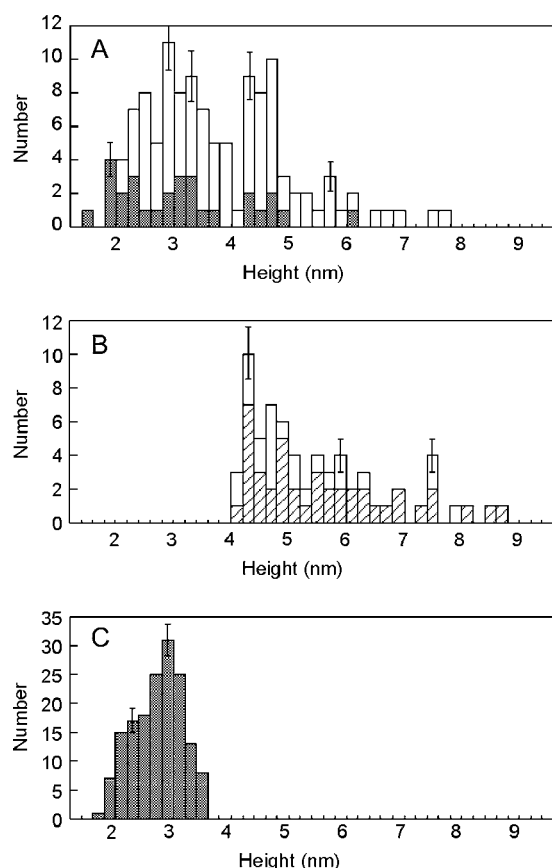
FIGURE 2 Heights of hSwi-Snf alone, heights of hSwi-Snf bound to chromatin near sites of significant remodeling, and nucleosome heights. Panel *A* shows the distribution of hSwi-Snf heights in images such as those in Fig. 1 *A*. The open bars are particles imaged only topographically. The solid bars are particles in topographic images for which a corresponding particle was found in a recognition image obtained by scanning using an AFM tip containing the BRG1 antibody. Only some of the topographic images were checked for recognition; thus the larger numbers of open bars do not reflect low recognition efficiency. The efficiency of BRG1 recognition in these images is estimated to be ∼60%. Panel *B* shows heights for particles identified as hSwi-Snf (height ≥4.2 nm, width and shape characteristic of hSwi-Snf; see text) in images of hSwi-Snf plus MMTV nucleosomal arrays that show major remodeling changes after ATP addition to the in situ sample. The striped bars are heights measured in images before the addition of ATP to the deposited samples and the open bars are heights after ATP addition. Panel *C* shows the height distribution for nucleosomes measured in all 18 high-resolution fields analyzed. Heights were measured in the −ATP image to avoid remodeling effects. The average height value for this set of nucleosomes is 2.7 ± 0.4 nm. In each of the three panels, the *y* axis is the number of particles (hSwi-Snf or nucleosomes) with a particular height value and the *x* axis is height, binned in 0.2-nm intervals. Error bars are ± 1 SD.

slightly higher than for the 4.5-nm class. Note that the distribution does not include all the (abundant) shorter particles, heights <2 nm, present in either the topographic or recognition images; the point here is to determine which particles are intact hSwi-Snf and particles <2 nm are too small to be intact complexes (see below).

Particle widths were also measured in the topographic images. Although width values are affected by "tip broadening," which is due to the finite size of the AFM probe, width measurements can provide supporting evidence and are particularly useful when comparing relative particle widths in the same image (see below). Widths of hSwi-Snf complexes with heights >3.0 nm usually fall in the 45–70-nm range; shorter particles typically have somewhat lower widths (data not shown). EM image reconstruction studies found that yeast Swi-Snf (28) and PBAF (29) are oblate in shape, i.e., one dimension is significantly smaller than the other two. PBAF, a BRG1-containing mammalian remodeling complex, is suggested to be an open C-shaped structure. Some of the complexes we observe, cf. 1 in Fig. 1 *C*, are similar in shape to some EM views of that complex.

The 4.5-nm high class of particles are probably intact complexes. For example, an average height value of ∼6 nm was measured for glutaraldehyde-fixed, air-dried hSwi-Snf complexes in the previous AFM study (17). That value is quite consistent with the height of our 4.5-nm class of particles because nucleosome heights averaged ∼4 nm in that study versus ∼3 nm here (see below). DNA-bound yeast Swi-Snf, imaged by EM approaches, showed width values (heights were not determined) in the same range as those of the 4.5-nm high complexes (16). Schnitzler et al. (17) measured widths of 30–40 nm for hSwi-Snf but their study used carbon nanotube tips, which have a higher resolution (and thus yield lower width values) than the standard tips used here. However, the relative nucleosome/hSwi-Snf widths in that study, 17:30–40, are similar to the width ratios for the 4.5-nm class of particles in our study, 24:45–70. The estimated volumes (height × area, assuming various geometries) of the 4.5-nm-high complexes relative to nucleosomes measured in the same images are also consistent with this particle being intact (2 Mda) hSwi-Snf (data not shown).

We also observe particles whose heights are greater than 5 nm. The previously noted particle asymmetry (oblate shape) may account for at least some of the particles in the 5–6-nm range; these particles often have smaller than typical width values for their heights suggesting that they may be complexes that have fallen on the surface such that a long axis of the complex lies in the vertical direction (cf. particle *9* in Fig. 1 *A*). The particles with heights >6 nm are likely to be aggregates of multiple smaller complexes. They usually exceed (sometimes by 150–200%) the characteristic width range for individual hSwi-Snf complexes (cf. particle *4* in Fig. 1 *A*) and the taller ones are highly irregular in shape, giving the appearance of being aggregated (not shown). Aggregates involving hSwi-Snf are also seen in the hSwi-

particles with heights >2 nm in these samples is estimated to be ∼60–70%. This is lower than the recognition efficiency in our previous studies (>90%) using histone antibodies (25). Lower recognition efficiency may be due to the presence of both BRG1 and BRM-containing complexes in our hSwi-Snf prep and/or to an enhanced possibility for antigenic sites to be buried in large complexes like these. For example, recognition efficiency for the 3-nm class of particles is

Snf+DNA and hSwi-Snf+chromatin images (see below). Previous studies imaged fixed hSwi-Snf in dried samples (16,17); here unfixed hSwi-Snf was imaged in solution. hSwi-Snf fixed as in the previous studies shows a range of particle heights, including shorter ones, but we also found an increase in the numbers and heights of very tall, clearly aggregated particles (up to 13 nm, data not shown). Thus, the use of fixed hSwi-Snf was avoided in these studies.

This analysis also detects a previously unreported feature in imaged remodeling complexes, low height, diffuse material extending out from the base of the complex in a particular direction (Fig. 1 C, complexes 1 and 5). The height of this projecting material is ~2 nm or less and it can vary in size and shape. Because the feature can be found on various sides of the particle in different images, it is not a result of the scanning process itself, which would produce a feature with a constant orientation relative to the scan direction. This projecting material can be found in complexes of various sizes and is also observed in the hSwi-Snf+chromatin images (see below).

General features of hSwi-Snf bound to chromatin

The imaging studies of isolated hSwi-Snf complexes provide a knowledge base to use in a search for these complexes in images of MMTV nucleosomal arrays plus hSwi-Snf (incubated together at 1:6 hSwi-Snf/chromatin molar ratios, then deposited and imaged in solution on GD-APTES mica). The analysis was focused specifically on those hSwi-Snf complexes found near the sites of major chromatin remodeling changes, i.e., complexes on arrays that underwent major structural alterations after the activation of hSwi-Snf by the addition of ATP to the deposited sample. That focus was made possible by our ability to image the very same molecules before and after ATP addition (18). Previous work using this approach established that the major chromatin structural changes observed after ATP addition reflect bona fide nucleosome remodeling events in individual molecules (see Wang et al. (18) for details of various controls). Supplemental Fig. 1 (Supplementary Material) shows one such control (not previously shown); the same MMTV chromatin molecules (no hSwi-Snf) imaged before and after ATP addition show no major chromatin structural changes. If hSwi-Snf were present, 5–10% of the chromatin molecules would show major changes (18).

Recognition imaging could not be used for hSwi-Snf identification in samples containing chromatin because BRG1 antibodies (several from different sources were tried) can also recognize nucleosomes (data not shown). Therefore, identification of hSwi-Snf complexes in the presence of chromatin will be based on criteria from topographic and recognition imaging of hSwi-Snf alone (Figs. 1 A and 2 A) but will involve topographic images (see below). The specific criteria used to identify these chromatin-bound hSwi-Snf are heights ≥4.2 nm, width values from 45 to 70

nm, and a shape that is not highly irregular (aggregated particles typically are irregular). Nucleosomes average 2.7 ± 0.4 nm in height (Fig. 2 C) and 24 ± 3 nm in width when measured in the same set of images in which hSwi-Snf complexes were identified. The hSwi-Snf criteria should thus exclude nucleosomes.

For the analysis, 94 areas showing significant chromatin changes after ATP addition were selected from low-resolution images (typically 5–10% of the molecules in such images show major changes after ATP is added (18)). From this set of 94, 18 pairs of image fields (− versus + ATP) containing particles that both fit the above size/shape criteria for hSwi-Snf and were located near sites of significant chromatin structural alterations after ATP addition were selected. These 18 were analyzed in detail in higher magnification images. The height distribution for the complexes in these 18 pairs of images is shown in Fig. 2 B. Heights were measured before and after ATP addition (striped and open bars, Fig. 2 B). Averaged over the whole data set, heights change only slightly after ATP addition. The occasional large changes observed are usually height decreases (cf. Fig. 3 A). Four specific examples from the set of images used to produce Fig. 2 B are presented in Fig. 3; these four examples will be discussed in detail below.

Many of these chromatin-bound complexes have heights of ~4.5 nm, the same average height value as intact hSwi-Snf complexes imaged alone, but there are also many taller complexes (Fig. 2 B). In the images, hSwi-Snf complexes typically appear to be incorporated into the associated nucleosomal array(s), with multiple DNA strands connecting the complex to the rest of the array (cf. Fig. 3, A, B, and D). This is by far the most common mode of hSwi-Snf/chromatin interaction in the data set, regardless of the height of the hSwi-Snf complex. It suggests that hSwi-Snf may lie on top of (or under) DNA or a nucleosome(s) in the arrays. A 2.4–4.8-nm-high hSwi-Snf complex (the major range of complex heights seen in Fig. 2 A) plus an associated nucleosome ~2.7 nm in height (Fig. 2 C) could produce particles ranging from ~5–8 nm in height. This range is consistent with the range of height values (from 5 to 8 nm) seen in Fig. 2 B, assuming heights of hSwi-Snf and a bound nucleosome are additive. Note that EM imaging of yeast Swi-Snf and human PBAF complexes (28,29) suggest modes of complex/nucleosome interaction in which heights of hSwi-Snf and a nucleosome to which it is bound may not be strictly additive. It is unlikely that these taller complexes in the chromatin images are simply the same types of taller complexes noted in Fig. 2 A because the chromatin-bound complexes maintain characteristic hSwi-Snf widths and are regular in shape (see below), unlike those taller complexes in Fig. 2 A. Whether hSwi-Snf lies on top of or under DNA or nucleosomes in the associated array(s) is very difficult to determine from this type of data. Other studies (R. Bash, H. Wang, C. Anderson, J. Yodh, G. Hager, S. Lindsay, and D. Lohr, unpublished data) have detected recognition signals from hSwi-Snf complexes when
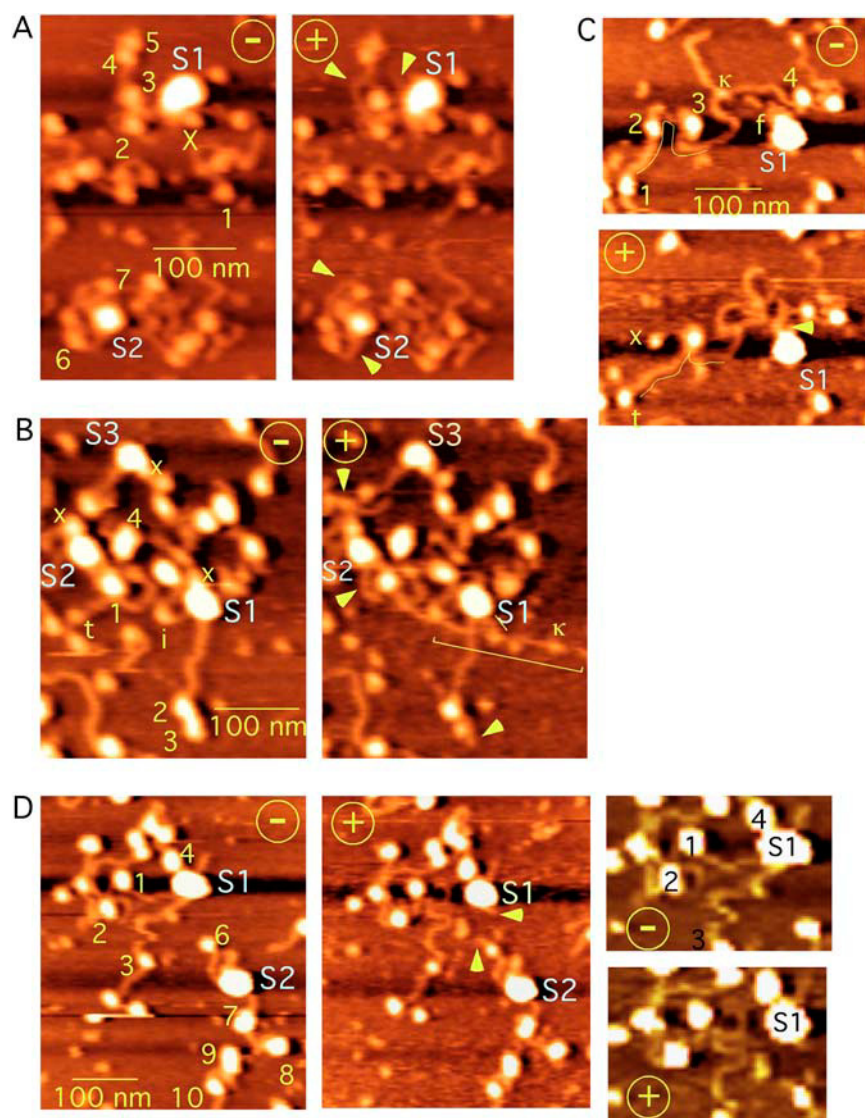
FIGURE 3 Examples of hSwi-Snf complexes bound to MMTV nucleosomal arrays and the remodeling events that occur near these identified complexes. Images of the same fields before (−) and after (+) in situ ATP addition to deposited hSwi-Snf + MMTV nucleosomal arrays are compared. The hSwi-Snf complexes identified in each pair of images (using the criteria described in the text) are designated as S1, S2, etc. Nucleosomes are numbered. Yellow arrows identify features involving DNA changes, such as newly released DNA, that are present after ATP addition. These various features are discussed in the text. The heights of the hSwi-Snf complexes shown in this figure are tabulated, − and + ATP, in Table 1 and the average nucleosome heights in the high-magnification image from which this example was taken are also given in Table 1. The pair of images to the immediate right of the +ATP image in panel D are from the region around S1 in image D, using an image presentation adjusted (contrast, etc.) to enhance DNA visibility. All samples shown in this figure were checked in this way to insure the correctness of the identified DNA paths. The leveling algorithm necessary to maximize contrast causes the dark horizontal streaks in these images. They are unavoidable but clear indications of taller particles. The middle streak in panel A is due to a tall complex just off right of the field shown.

scanning hSwi-Snf+chromatin samples with histone-tethered AFM tips. Such signals could reflect a nucleosome(s) lying on top of a hSwi-Snf complex.

Thirteen of the 18 high magnification fields contained more than one hSwi-Snf complex (cf. Fig. 3, A and D), with several containing three to five (cf. Fig. 3 B). These high magnification fields were small, containing only a few (from 2–10) array molecules. Also, complexes are often associated with linked or coalesced (Fig. 3, A, B, and D) array molecules and multiple, but distinct, complexes can even be found on the same set of coalesced arrays (cf. Fig. 3 B). These tendencies are also illustrated in Supplemental Fig. 2 (leftmost and rightmost panels) (Supplementary Material). They greatly complicate the detailed analysis of remodeling changes, especially in tracing the DNA path over extensive distances (see below).

Based on the studies of hSwi-Snf alone (Figs. 1 A and 2 A), it is likely that these images also contain hSwi-Snf

(BRG1-containing) complexes with heights <4 nm. They would be difficult to distinguish unambiguously from nucleosomes because their widths also tend to be diminished compared to the larger complexes. These short complexes can contain the catalytic subunit BRG1 (Fig. 2 A) and therefore are capable of remodeling. The original data set from which the 18 image pairs with identifiable hSwi-Snf (heights >4 nm, etc.) were chosen also contained pairs of images in which significant remodeling changes were observed but no complex of height >4 nm was present. Some of those (and some of the 18 fields with identifiable hSwi-Snf complexes) did contain one or two particles with heights just less than 4 nm (3.8 and 3.9 nm) and widths slightly greater than a typical nucleosome (not shown); these could be hSwi-Snf complexes. In addition, we initially expected to observe many examples of hSwi-Snf present before but not after ATP addition, leaving behind a remodeled nucleosomal array, but the only cases in which this was observed (three) involved

particles with heights less than 4 nm. In contrast, all hSwi-Snf complexes of height greater than 4 nm (in the entire data set) were found in the same position before and after ATP addition (cf. Fig. 3, *A–D*), despite the clear occurrence of remodeling changes in the nearby or associated arrays. Whether this indicates that hSwi-Snf is tethered to the surface (as is the chromatin) is uncertain.

We also observe (a few) hSwi-Snf complexes that fit the size criteria but are bound to chromatin arrays that show no chromatin changes after ATP addition. Those complexes have heights that are similar to the heights of the complexes in Fig. 2 *B* (data not shown). We also observe aggregated particles that probably involve hSwi-Snf because such aggregates are not seen in these chromatin samples without hSwi-Snf (cf. Supplemental Fig. 1; Supplementary Material). Those particle heights (and widths) are much larger than any shown in Fig. 2 *B* and include the huge aggregated particles described previously (17,18).

The rest of the analysis will focus on the complexes ≥4.2 nm in height that are located near major remodeling changes. The similarities of their widths to bona fide (BRG1-containing) hSwi-Snf complexes, even when their heights are greater, argues that we are observing discrete complexes not aggregates. The complexes are significantly larger than nucleosomes measured in the same images and even when hSwi-Snf partially overlaps shorter particles (probably nucleosomes), which is common in the data set (Fig. 3, *A* and *B*), the two types of particles retain clear height differentials. These features taken together indicate that the particles we have identified in the chromatin images are hSwi-Snf complexes. Moreover, these types of particles are not present in images of MMTV chromatin without hSwi-Snf (Supplemental Figs. 1 and 2; Supplementary Material). They can often be identified by inspection in low magnification images because of their heights.

Specific examples illustrating hSwi-Snf/chromatin interactions and remodeling changes

To illustrate the types of interactions and remodeling events observed in arrays containing bound hSwi-Snf, four pairs of images are presented (Fig. 3, *A–D*). For each pair, we first identify the hSwi-Snf complex(es), discussing their relationship to the array. We then go on to discuss the types of remodeling events seen upon ATP addition and suggest mechanisms by which the associated hSwi-Snf complex may have brought about those changes. Obviously, it is not possible to prove that the chromatin changes observed were produced by the bound hSwi-Snf complex, although in two examples, the nature of the changes indicate that the bound complexes are involved (Fig. 3, *C* and *D*). There is no attempt to analyze every array molecule in an image or the many minor changes that occur and it is not always possible to be sure of the exact nature of remodeling events even though major chromatin changes are clearly observed.

Images *A*

hSwi-Snf chromatin interactions

The two identified complexes in this image, S1 and S2, are significantly taller than nucleosomes in this same image (Table 1) and their widths (50–65 nm) fall in the range seen for intact hSwi-Snf complexes imaged alone, whereas the nucleosomes in this image average 23 ± 3 nm in width. Thus, S1 and S2 are almost certainly hSwi-Snf complexes. Each complex has multiple DNA strands (presumably double strands) or small particle contacts appearing to enter the complex from various directions, suggesting that the complex is bound to, lying on or under, DNA or a nucleosome(s) in the array(s) with which it is associated. S1 contacts a short (2.1 nm), discrete particle (× in the −ATP image) whose height value is similar to the heights of H3-H4 tetramer-DNA particles measured under these solution conditions (data not shown). There are probably two nucleosomal array molecules involved with each of the hSwi-Snf complexes in this image, based on the measured chromatin contour lengths and numbers of associated nucleosomes. Such linking of arrays is very common in the data set.

Remodeling changes

This image pair illustrates DNA release in specific regions while other regions remain unchanged.

S1. After ATP addition, there is roughly 45 nm (130 bp) more DNA in the vicinity of nucleosome 3 (*yellow arrow*, +ATP image); this released DNA could come from one of the nearby nucleosomes. For example, nucleosomes 4 and 5 show ~25% height decreases after ATP addition. S1 has released ~22 nm (65 bp) of DNA after ATP addition (*yellow arrow* at top of *S1*, +ATP image).

S2. Newly released DNA (11 nm (~30 bp) and 15 nm (~45 bp)) appears after ATP addition in the vicinity of

TABLE 1 hSwi-Snf and nucleosome height values for each of the examples in Fig. 3

Image	hSwi-Snf height −ATP (nm)	hSwi-Snf height +ATP (nm)	Average nucleosome heights (nm)*
A:S1	7.4	6.0	2.4 ± 0.4
S2	5.4	5.0	
B:S1	5.0	5.0	2.5 ± 0.3
S2	4.3	4.3	
S3	4.3	4.2	
C:S1	6.2	6.2	2.6 ± 0.3
D:S1	7.2	7.6	2.7 ± 0.4
S2	7.5	7.5	

*Note that the high magnification fields from which Fig. 3, *A–D*, are taken are larger than the images shown. Thus, more nucleosomes than are present in the images were measured to obtain the above values. That nucleosome data were originally divided into nucleosomes in array molecules containing hSwi-Snf and those in arrays that did not. There was no difference between the two sets of heights so they were combined to obtain the above values. Nucleosome heights shown were measured in the −ATP images to avoid remodeling effects.

nucleosomes 6 and 7, respectively (*yellow arrows*, +ATP image). Nucleosome 6 is ~25% shorter, which could account for the 30-bp release, but the source of the 45 bp released from the nucleosome 7 region is unclear.

Images *B*

hSwi-Snf chromatin interactions

Again, the heights (Table 1) and widths (45–60 nm) of the three suggested hSwi-Snf complexes, S1, S2, and S3, are significantly different from nucleosome heights and nucleosome widths (26 ± 2 nm) measured in this image. There are an indeterminate number of chromatin molecules involved with these three complexes and each of the three complexes appears to be incorporated into the chromatin organization. S1 and S2 have three or more DNA strands/particle contacts (and S3 has at least two) disappearing into the complex from several directions and each of the three complexes partially overlaps or contacts a short, discrete particle (× in the −ATP image), whose height is similar to that of an H3-H4 tetramer-DNA complex. The short particle near S1 disappears after ATP addition and those near S2 and S3 show slight height decreases. Heights of the hSwi-Snf complexes do not change after ATP addition (Table 1). Particle 4 (height = 2.9 nm) may be two nucleosomes lying very close together.

Remodeling changes

This image pair illustrates the most dramatic type of remodeling event we observe, the establishment of new DNA paths including the de novo appearance of a substantial length of DNA (*long yellow bracket*, +ATP image), in this case >200 nm, after ATP addition. Such activities have not been previously suggested for ATP-dependent nucleosome remodeling complexes. Small "knobs" are often observed at intervals along the released DNA (κ, +ATP image). Their heights, ~1 nm, suggest proteins (hSwi-Snf subunits, histones, or BSA); such knobs can also be found free of DNA (cf. −ATP image).

The long stretch of DNA appearing after ATP addition is probably composed of several segments from various places rather than one long stretch from a single source. For example, DNA entering S1 from the short particle i in the −ATP image is apparently gone after ATP addition and DNA from i passes below S1 (and across another DNA) and appears to contact DNA extruded from S1 (*yellow line below and to the* right *of S1*, +ATP image). After ATP addition, a new loop of 33 nm (100 bp) of DNA appears between S2 and nucleosome 1 (*yellow arrow*, +ATP image) and a 62-nm stretch of DNA from nucleosome 1 to an apparent terminus (t, −ATP image) has disappeared. The 62-nm stretch could have swung toward S1 to contact the short particle i (the distance from nucleosome 1 to particle i in the −ATP image is ~65 nm, i.e., about this same length) or swung up to

make contact with S2, accounting for the new loop. Between S2 and S3, new material (DNA and protein) appears after ATP addition (*yellow arrow*, +ATP image), probably originating from a large amorphous glob just to the left of this image field. Again, parts of these array molecules remain unchanged.

There are also chromatin changes that occur at a significant distance from S1 but on DNA that is clearly connected to it; ~25–30 nm (75–90 bp) of DNA appears near (terminal) nucleosome 3 after ATP addition and nucleosome 3 is ~50% shorter. Nucleosome 2, adjacent to 3, is unchanged in height.

Images *C*

hSwi-Snf Chromatin Interactions

S1, the lone complex in this image, is quite different in size from nucleosomes (Table 1). S1 also shows the novel feature seen in images of hSwi-Snf alone (Fig. 1 *C*), a low (~1 nm) projection (*f* in the −ATP image). This projection extends toward the nearby DNA but does not appear to contact it in the absence of ATP but clearly does so after ATP addition (*yellow arrow*, +ATP image). This difference suggests that we have detected hSwi-Snf making contact with a chromatin molecule in these two images. S1 shows no height change after ATP addition. Two array molecules appear to be linked together in this field; an ~1.3-nm knob (κ in the −ATP image) apparently serves to link them. This knob has moved after ATP addition.

Remodeling changes

There are radical topology changes in the DNA located near S1 after ATP addition; it is formed into loops and there is ~66 nm more DNA in the region between nucleosomes 3 and 4 (including that projecting above κ in the −ATP image). There are also significant DNA path changes in the nucleosome 1–3 region after ATP addition. For example, DNA now appears to pass directly from nucleosome 1 to 3, having been completely released from nucleosome 2 (compare *thin lines* − versus + ATP images). A particle remains at the original position of 2 (shorter by ~30% and no longer on the DNA path) after ATP addition, probably due to the tethering of those histones to the surface. Surface-bound histones could also be observed after salt-induced release of DNA from tethered nucleosomal arrays (22,24). After ATP addition, nucleosome 1 resides at the DNA terminus (t in the +ATP image), an apparent movement of 27 nm (80 bp) on the DNA, and DNA appears to have been pulled toward S1 (compare *thin yellow lines* in the − versus + ATP image). For example, the distance from the array terminus (t in the +ATP image) to nucleosome 3 is ~65 nm shorter after ATP addition, i.e., equal to the length increase (~66 nm) in the nucleosome 3–4 region (see above). Thus, there has apparently been a redistribution of DNA toward S1. Nucleosomes 3 and 4 are ~30% shorter after ATP addition.

Images *D*

hSwi-Snf chromatin interactions

The hSwi-Snf candidates in this image, S1 and S2, have heights (Table 1) and width values (50–65 nm versus 24 $\pm$ 3 nm for nucleosomes) that differ significantly from the nucleosomes in the image. Both complexes have multiple DNA strands entering into them from various directions and thus again appear to be integral parts of the associated arrays. There are at least two array molecules involved with S1 (and perhaps with S2). Despite a major DNA path change around S1 (see below), the heights of both complexes are unchanged after ATP addition (Table 1).

Remodeling changes

S1. Before ATP addition, DNA from nucleosome 3 passes through S1 then to nucleosome 1. After ATP addition, DNA from nucleosome 3 is no longer entering S1 but appears to go directly toward (and into) nucleosome 1. The total length of DNA in this region is ~30–35-nm greater after ATP addition. Thus, there has been a change in path involving release of ~90–100 bp of DNA from somewhere, perhaps from S1, a nucleosome(s) bound on or under S1 or from nucleosomes 1 and/or 3, both of which are shorter (1 by 20% and 3 by 33%). Images adjusted to show DNA features more clearly are shown immediately to the right of *D*. After ATP addition, an ~55 nm (160 bp) loop on the right side of nucleosome 2 has apparently disappeared and roughly 20 nm (60 bp) of DNA is extruded from S1 (*yellow arrow*, +ATP image).

S2. In the array containing S2, ATP addition results in ~23 nm (70 bp) of DNA being released from nucleosome 6 (*yellow arrow*, +ATP image). Nucleosomes 6–9 are ~20% shorter after ATP addition. There also appear to be DNA path changes around nucleosomes 7–10 but they are difficult to define. Particles 7 and 9 may be dinucleosomes.

In previous work, DNA release (''unwrapping'') from nucleosomes was one of the most common types of remodeling changes observed and one that was shown to be remodeling specific (18). DNA release is also very common in this data set (cf. Fig. 3, *A–D*). Fig. 4 presents a histogram of the lengths of DNA release for the set of 18 high-resolution fields analyzed in detail here. As previously, the data identify a preference for release of roughly one nucleosomal turn of DNA (80 bp) but also finds evidence for another peak in the distribution, averaging around 40 bp.

The pair of images in Fig. 5 suggest a feature thought to occur during nucleosome sliding mediated by remodeling complexes (3,9). The changes in DNA length to the terminus and the appearance of a second DNA region projecting from the nucleosome after ATP addition are consistent with a bulge of DNA propagating around the nucleosome in association with a nucleosome sliding event (see Fig. 5 legend). Such bifurcated structures were observed in two other molecules
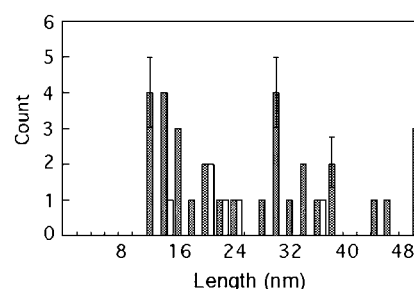

FIGURE 4 The lengths of DNA released during remodeling events. The lengths of DNA released in remodeling events, from either terminal (*open bars*) or internal nucleosomes (*solid bars*), for the entire set of 18 high-resolution images are shown versus the number of times that release length was observed in the data set. These lengths were obtained by measuring DNA pathlengths before and after ATP addition. Values were binned in 2-nm intervals. Error bars are $\pm$ 1 SD.

undergoing sliding in the original (94) set of areas showing changes after ATP addition.

Imaging hSwi-Snf Plus MMTV DNA

To characterize the interactions of hSwi-Snf with naked DNA, the complex was incubated with the same DNA used to reconstitute MMTV nucleosomal arrays, at several molar ratios (1:1, 1:2; 1:3, and 1:6, hSwi-Snf/DNA), deposited as usual on GD-APTES mica and imaged. At the ratios used in the chromatin analyses (1:6), there are few hSwi-Snf/DNA complexes per field, the fields contain mostly free DNA, and the particles that are found on DNA in these images are typically very short, with multiple (short) particles often closely associated (Fig. 1 *E*). At higher (1:1) hSwi-Snf/DNA ratios, more DNA-bound particles are found (Fig. 1 *D*) but again, most are short, although there are also some taller particles. The taller particles typically appear as multiple (but distinguishable) particles lying close to one another or as irregularly shaped particles (cf. particle *3*, Fig. 1 *D*) that are almost certainly aggregates. The widths of some of these large particles can be over twice the width of intact (~4.5 nm) hSwi-Snf complexes. The height distribution for
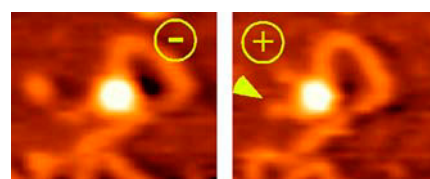
FIGURE 5 Possible bulge propagation during a nucleosome sliding event. After ATP addition, the nucleosome in this image has slid almost to the adjacent DNA terminus (with no other change in the rest of the molecule; not shown) and the DNA now appears bifurcated on the left side of the nucleosome with the lower ''branch'' (*yellow arrow*, +ATP image) broader than the upper. This breadth could reflect a doubled ''bulge'' of DNA; if doubled, its length (25 nm $\times$ 2 = 50 nm) equals the difference in length from this nucleosome to the DNA terminus in the − versus + ATP images. Thus, this branch could be a trapped bulge of DNA generated during nucleosome sliding.

DNA-bound particles, from all ratios of hSwi-Snf/DNA analyzed, shows that a majority are <3 nm in height (*open bars*), with a peak at ~2 nm, plus a few taller particles (*striped bars*, Fig. 6). This height distribution is quite different from that of chromatin-bound hSwi-Snf (Fig. 2 *B*), indicating that hSwi-Snf interactions with DNA and chromatin differ at least in the sizes of bound complexes. The scarcity of complexes, especially at low (1:6) hSwi/Snf/DNA ratios, could reflect a decreased binding strength between DNA and hSwi-Snf compared to chromatin and hSwi-Snf. However, we cannot exclude the possibility that differential adsorption of DNA/hSwi-Snf (versus chromatin/hSwi-Snf) could also contribute to the low frequency of observed complexes, even though DNA seems to bind well to this surface (data not shown). These results were surprising and we have repeated them many times at the various hSwi-Snf/DNA ratios, using the same concentrations and hSwi-Snf samples used in the analyses of chromatin+hSwi-Snf or hSwi-Snf alone and treating samples in the same way (Experimental Procedures). Again, imaging was done in solution with unfixed hSwi-Snf/ DNA complexes, conditions not used in previous imaging studies of Swi-Snf bound to DNA. Recognition imaging with the BRG1 antibody confirms that any size DNA-bound particle can contain BRG1 (data not shown).

Applying the same approach used to study ATP-induced changes in MMTV nucleosomal arrays, we checked for ATP-induced changes in the DNA/hSwi-Snf complexes. Surprisingly, no changes in DNA or hSwi-Snf were detected. This result was confirmed in several experiments, using different hSwi-Snf concentrations. It is possible that modest, undetected (by AFM) changes are occurring and/or the highly coiled/entangled nature of DNA in most of these complexes prevents the detection of changes. However, some molecules are extended enough to provide a clear test and we saw no changes in any of these (cf. Fig. 1 *E*). Thus, results obtained with DNA/hSwi-Snf complexes again differ from those obtained with chromatin/hSwi-Snf complexes, even though both were analyzed in the same way and under as similar conditions as possible.
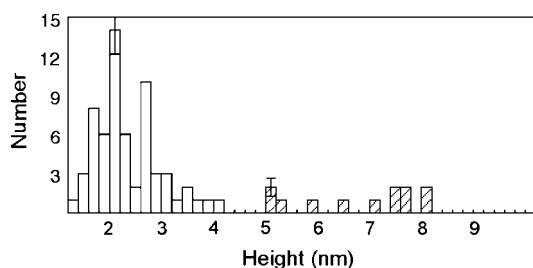

FIGURE 6 The particle height distribution for hSwi-Snf bound to DNA. This figure shows the histogram of heights measured for hSwi-Snf complexes bound to MMTV promoter DNA. Only particles actually bound to DNA were included. The *y* axis is the number of particles with a particular height value and heights are binned in 0.2-nm intervals. Data from all stoichiometries of hSwi-Snf/DNA (see text) are included. Error bars are ± 1 SD.

DISCUSSION

Topographic and recently developed recognition imaging AFM approaches were used to characterize the human Swi-Snf (hSwi-Snf) ATP-dependent nucleosome remodeling complex in solution. This knowledge was then used to locate, in topographic images, complexes bound to MMTV promoter nucleosomal arrays that underwent major structural changes after hSwi-Snf activation (ATP addition) in situ. An approach that can image the same individual molecules before and after the addition of ATP to the sample was used (18). Features of the hSwi-Snf/chromatin interaction and of remodeling were analyzed. Similar studies of hSwi-Snf interactions with naked MMTV DNA were carried out. The analyses reveal novel information about the hSwi-Snf complex, its interactions with DNA or chromatin, and its remodeling activities.

hSw-Snf/chromatin interactions

1. hSwi-Snf complexes typically appear to be incorporated into chromatin arrays, with multiple DNA strands emanating in different directions from a bound complex, thus connecting the complex to the rest of the array(s). After ATP addition, the positions of the DNA emanating from the complex sometimes change (Fig. 3 *D*) and release of new DNA from the complex can occur (Fig. 3, *A–D*). The mode of hSwi-Snf/chromatin binding seems likely to involve hSwi-Snf lying on top of or under DNA or a nucleosome(s) of the array; the latter could account for the higher incidence of taller complexes in the chromatin images (Fig. 2 *B*) versus hSwi-Snf alone (Fig. 2 *A*).
2. An individual hSwi-Snf complex is often associated with multiple nucleosomal array molecules, − or + ATP. These multiple chromatin arrays often are in close contact or even coalesced together. This could account for the multiplicity of DNA strands typically observed entering the complex. It is also possible that hSwi-Snf/chromatin association involves the formation of loops as observed previously (16). Observing multiple hSwi-Snf complexes in a small area is common, sometimes even on the same set of coalesced array molecules (cf. Fig. 3 *B*).
3. Images of hSwi-Snf plus naked MMTV DNA show some differences (fewer complexes, shorter particles) compared to chromatin plus hSwi-Snf. These differences for DNA and chromatin samples treated similarly indicate some differences in hSwi-Snf interactions with the two substrates. Presumably the histone component is responsible for this difference.

Remodeling changes

The types of events observed here after ATP addition are, or should produce, the types of changes suggested from biochemical studies of remodeling (nucleosome sliding, DNA

dissociation from nucleosomes, topological changes, dinucleosome formation, DNA transfer between octamers).

1. Multiple and differing kinds of remodeling events can occur in close proximity, sometimes even on the same molecule (Fig. 3, *B* and *D*). Thus, hSwi-Snf action is inherently heterogeneous and single-molecule approaches will be required for a full understanding of its actions. Ensemble-average biochemical studies have also indicated that hSwi-Snf action is heterogeneous (30).

2. In our studies, remodeling never involves entire arrays; a part(s) always appears unchanged. In fact, alterations were often at the level of specific individual nucleosomes (Fig. 3, *A–D*). Thus, hSwi-Snf is not highly processive under these conditions (see also Martens and Winston (6) and Flaus and Owen-Hughes (7)). Such specificity is also consistent with recent biochemical results showing that hSwi-Snf can remodel neighboring nucleosomes on MMTV promoter arrays differently (31).

3. Decreases of 25–50% in nucleosome heights (Fig. 7) are commonly observed after ATP addition (hSwi-Snf activation). The heights of these shortened (post-ATP addition) nucleosomes are similar to heights of H3-H4 tetramer/DNA particles (data not shown), which suggests (but does not prove) histone H2A-H2B loss from these nucleosomes upon remodeling. H2A-H2B loss has recently been shown to occur during ATP-dependent nucleosome remodeling (7), including MMTV promoter remodeling by hSwi-Snf (31). Moreover, we have demonstrated H2A-H2B loss during remodeling of these MMTV arrays, using a recognition imaging approach (R. Bash, H. Wang, C. Anderson, J. Yodh, G. Hager, S. Lindsay, and D. Lohr, unpublished data). In addition, nucleosomes that show height decreases after ATP addition often lie near sites of partial DNA release, which is also consistent with histone loss. The hSwi-Snf complex is also commonly observed to partially overlap particles with the heights of short (potentially histone-depleted) nucleosomes, even before ATP addition (cf. Fig. 3 *B*).

4. DNA release from nucleosomes is a common remodeling event, with two preferences for partial release, ~15 nm (40–50 bp) and ~30 nm (80–90 bp), detected in the (limited) set of examples analyzed here (Fig. 4). The ~80-bp preference was previously observed in a larger data set from a general analysis of MMTV chromatin remodeling (18); 80 bp corresponds roughly to one nucleosomal turn and is thus easy to rationalize in terms of nucleosome structure. The preference to release ~40 bp might be related to histone loss (see above).

5. The data set contains many examples of changes (nucleosome height decreases, DNA release, etc.) that occur at a distance from a hSwi-Snf complex bound to that chromatin molecule. Although it cannot be proven that the bound complex (and not a freely diffusing hSwi-Snf)
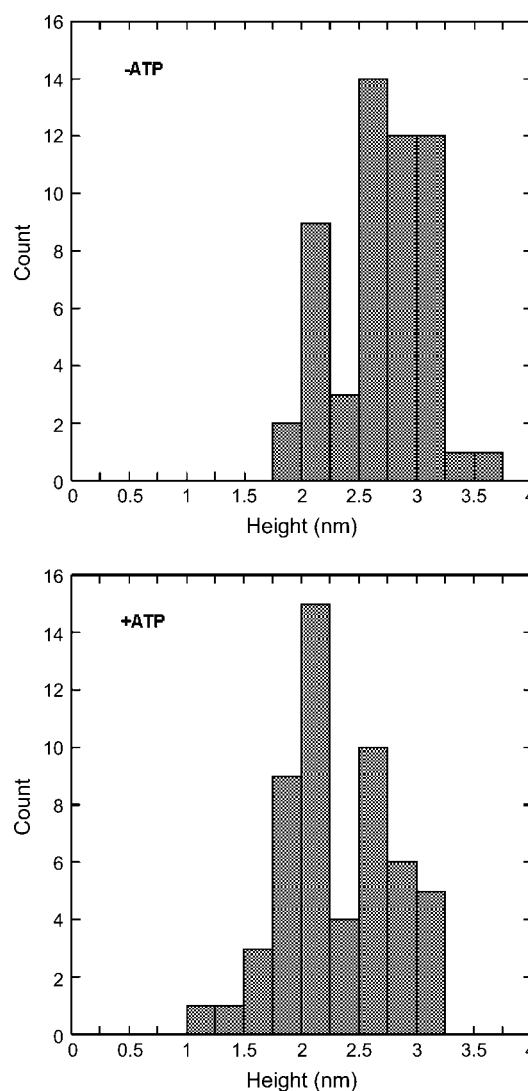
FIGURE 7 Nucleosome height decreases after ATP addition. Histograms of nucleosome heights before (*A*) and after (*B*) ATP addition for the images analyzed in Fig. 3 are shown. Values are binned in 0.25-nm intervals. The peak falls from just below 3 nm in the −ATP images to just above 2 nm in the +ATP images, an average decrease of ~25%.

caused the changes, in at least some cases the chromatin-bound complex is likely to be involved (Fig. 3 *B* and *D*). Thus, hSwi-Snf may be able to act from a distance, even in linear arrays. Remodeling complexes have been suggested to apply torsional stress to DNA, for example, by DNA twisting (3,6,7,32), and thus should be able to cause changes at a distance from the complex.

Complexes remain in the same position − or + ATP, even though major remodeling changes have occurred within the molecule(s) to which they are bound. No examples were found of a hSwi-Snf complex (height ≥4.2 nm, etc.) that was present in the −ATP image but absent in the +ATP image, leaving behind an altered nucleosomal array. The surface used in these studies

reacts with lysines and thus might also be able to tether hSwi-Snf to the surface. If there is tethering of even a fraction of hSwi-Snf complexes to the surface, it could explain why we see only 5–10% of the molecules in a field of chromatin molecules undergoing significant remodeling.

We also find examples of major remodeling changes in molecules containing only nucleosome-size particles, as well as examples of sub-4-nm particles that are present before but not after ATP addition, leaving behind remodeled chromatin. Whether these examples reflect the action of a hSwi-Snf complex that has come and gone after ATP addition or the action of chromatin-bound hSwi-Snf (BRG1-containing) complexes that are in the size range of nucleosomes cannot be determined.

7. hSwi-Snf bound to naked MMTV DNA does not carry out any AFM-detectable alterations when ATP is added, in contrast to chromatin, where the complex can produce significant change. These results suggest that ATP-induced remodeling changes that significantly affect DNA (path changes, release from nucleosomes, etc.) may depend on histone presence.

Surface effects are a constant concern in AFM studies, particularly when molecules are surface tethered, as is the case here. The possible impacts of surface effects on the results presented here should vary. In the studies of hSwi-Snf alone and of its binding to DNA or chromatin, AFM is being used as an analytical tool to score the populations of molecules in various states of complex formation in a solution of hSwi-Snf, hSwi-Snf plus DNA, or hSwi-Snf plus chromatin. The interactions that determine the population features occur in solution before deposition of components on the surface. Because it is not involved during the (solution) interaction processes, the surface should have a minimal affect on these population features. Differential absorption effects could impact the results but because each of the individual components (DNA, hSwi-Snf, MMTV chromatin) deposit and image satisfactorily, these effects are likely to be minor. EM has been used as an analytical tool in this way for some time, including studies of remodeling complexes and remodeling changes (16), and so has AFM (17). The studies presented here have the significant advantage that the imaging takes place in solution, thus avoiding artifacts associated with dehydration during deposition and imaging.

Surface effects are much more likely to impact the remodeling results. We often observe larger-scale changes than many suggested from ensemble-average biochemical studies (3,6,7). In part, this probably reflects our ability to assess remodeling changes on the same individual molecules at single-molecule resolution (see Wang et al. (18) for a more detailed discussion) and our choice to focus on significant alterations, due to AFM resolution considerations. However, surface features and surface tethering undoubtedly have effects on the remodeling features we observe. For example, tethering of nucleosomes to the surface may at least transiently strengthen their ability to create a local topologically closed domain (33), leading to enhanced torsional stress within that region when hSwi-Snf is active. Also, the lack of hSwi-Snf movement after ATP activation may be due to tethering of the complex to the surface; this would impact processivity and perhaps enhance the tendencies for hSwi-Snf action at a distance. However, the similarities in the kinds of changes observed here (nucleosome sliding, DNA release, etc.) to those detected in biochemical studies suggests that the effects of the surface on remodeling events may be quantitative rather than qualitative. At the other extreme, dilute solutions provide an environment with known and serious shortcomings in mimicking in vivo conditions (34).

Based on earlier results, we suggested that hSwi-Snf can approach and interact with nucleosomes via the 11-nm histone face (18). As shown here, the binding of hSwi-Snf to nucleosomal arrays probably involves it lying on or under DNA or a nucleosome(s) in the arrays. Nucleosomes usually lie flat on the surface in these images (based on height values). Thus, a hSwi-Snf complex lying on top of such a nucleosome would probably be interacting with the 11-nm face. hSwi-Snf is also observed to partially overlap nucleosomes whose heights indicate that they are lying flat on the surface. However, we also detected major DNA release from nucleosomes to which hSwi-Snf was not binding directly, including some at a considerable distance from the complex (Fig. 3, *A*, *B*, and *D*). Assuming that the changes did not result from a freely diffusing hSwi-Snf, this observation would indicate that hSwi-Snf can remove significant amounts of nucleosomal DNA (cf. 80 bp) without interacting directly with the nucleosome. Apparently, as suggested previously (6,9,18), remodeling complexes not only cause a variety of structural changes but can carry out these changes in different ways.

SUPPLEMENTARY MATERIAL

An online supplement to this article can be found by visiting BJ Online at http://www.biophysj.org.

REFERENCES

1. Peterson, C. L., and J. L. Workman. 2000. Promoter targeting and chromatin remodeling by the SWI/SNF complex. *Curr. Opin. Genet. Dev.* 10:187–192.

2. Narlikar, G. J., H. Y. Fan, and R. E. Kingston. 2002. Cooperation between complexes that regulate chromatin structure and transcription. *Cell.* 108:475–487.

3. Becker, P. B., and W. Horz. 2002. ATP-dependent nucleosome remodeling. *Annu. Rev. Biochem.* 71:247–273.

4. Peterson, C. L. 2002. Chromatin remodeling: nucleosomes bulging at the seams. *Curr. Biol.* 12:R245–R247.

5. Tsukiyama, T. 2002. The in vivo functions of ATP-dependent chromatin-remodelling factors. *Nat. Rev. Mol. Cell Biol.* 3:422–429.

6. Martens, J. A., and F. Winston. 2003. Recent advances in understanding chromatin remodeling by Swi/Snf complexes. *Curr. Opin. Genet. Dev.* 13:136–142.

7. Flaus, A., and T. Owen-Hughes. 2004. Mechanisms for ATP-dependent chromatin remodelling: farewell to the tuna-can octamer? *Curr. Opin. Genet. Dev.* 14:165–173.

8. Imbalzano, A. N., and H. Xiao. 2004. Functional properties of ATP-dependent chromatin remodeling enzymes. *Adv. Protein Chem.* 67:157–179.

9. Langst, G., and P. B. Becker. 2004. Nucleosome remodeling: one mechanism, many phenomena? *Biochim. Biophys. Acta.* 1677:58–63.

10. Shen, X., G. Mizuguchi, A. Hamiche, and C. Wu. 2000. A chromatin remodelling complex involved in transcription and DNA processing. *Nature.* 406:541–544.

11. Collins, N., R. A. Poot, I. Kukimoto, C. Garcia-Jimenez, G. Dellaire, and P. D. Varga-Weisz. 2002. An ACF1-ISWI chromatin-remodeling complex is required for DNA replication through heterochromatin. *Nat. Genet.* 32:627–632.

12. Damelin, M., I. Simon, T. I. Moy, B. Wilson, S. Komili, P. Tempst, F. P. Roth, R. A. Young, B. R. Cairns, and P. A. Silver. 2002. The genome-wide localization of Rsc9, a component of the RSC chromatin-remodeling complex, changes in response to stress. *Mol. Cell.* 9:563–573.

13. Hara, R., and A. Sancar. 2002. The SWI/SNF chromatin-remodeling factor stimulates repair by human excision nuclease in the mononucleosome core particle. *Mol. Cell. Biol.* 22:6779–6787.

14. Ura, K., and J. J. Hayes. 2002. Nucleotide excision repair and chromatin remodeling. *Eur. J. Biochem.* 269:2288–2293.

15. Gaillard, H., D. J. Fitzgerald, C. L. Smith, C. L. Peterson, T. J. Richmond, and F. Thoma. 2003. Chromatin remodeling activities act on UV-damaged nucleosomes and modulate DNA damage accessibility to photolyase. *J. Biol. Chem.* 278:17655–17663.

16. Bazett-Jones, D. P., J. Cote, C. C. Landel, C. L. Peterson, and J. L. Workman. 1999. The SWI/SNF complex creates loop domains in DNA and polynucleosome arrays and can disrupt DNA-histone contacts within these domains. *Mol. Cell. Biol.* 19:1470–1478.

17. Schnitzler, G. R., C. L. Cheung, J. H. Hafner, A. J. Saurin, R. E. Kingston, and C. M. Lieber. 2001. Direct imaging of human SWI/SNF-remodeled mono- and polynucleosomes by atomic force microscopy employing carbon nanotube tips. *Mol. Cell. Biol.* 21:8504–8511.

18. Wang, H., R. Bash, J. G. Yodh, G. Hager, S. M. Lindsay, and D. Lohr. 2004. Using atomic force microscopy to study nucleosome remodeling on individual nucleosomal arrays in situ. *Biophys. J.* 87:1964–1971.

19. Yoshinaga, S. K., C. L. Peterson, I. Herskowitz, and K. R. Yamamoto. 1992. Roles of SWI1, SWI2, and SWI3 proteins for transcriptional enhancement by steroid receptors. *Science.* 258:1598–1604.

20. Muchardt, C., and M. Yaniv. 1993. A human homologue of Saccharomyces cerevisiae SNF2/SWI2 and Drosophila brm genes potentiates transcriptional activation by the glucocorticoid receptor. *EMBO J.* 12:4279–4290.

21. Fryer, C. J., and T. K. Archer. 1998. Chromatin remodelling by the glucocorticoid receptor requires the BRG1 complex. *Nature.* 393:88–91.

22. Bash, R., H. Wang, J. Yodh, G. Hager, S. M. Lindsay, and D. Lohr. 2003. Nucleosomal arrays can be salt-reconstituted on a single-copy MMTV promoter DNA template: their properties differ in several ways from those of comparable 5S concatameric arrays. *Biochemistry.* 42:4681–4690.

23. Fletcher, T. M., B. W. Ryu, C. T. Baumann, B. S. Warren, G. Fragoso, S. John, and G. L. Hager. 2000. Structure and dynamic properties of a glucocorticoid receptor-induced chromatin transition. *Mol. Cell. Biol.* 20:6466–6475.

24. Wang, H., R. Bash, J. G. Yodh, G. L. Hager, D. Lohr, and S. M. Lindsay. 2002. Glutaraldehyde modified mica: a new surface for atomic force microscopy of chromatin. *Biophys. J.* 83:3619–3625.

25. Stroh, C., H. Wang, R. Bash, B. Ashcroft, J. Nelson, H. Gruber, D. Lohr, S. M. Lindsay, and P. Hinterdorfer. 2004. Single-molecule recognition imaging microscopy. *Proc. Natl. Acad. Sci. USA.* 101:12503–12507.

26. Hinterdorfer, P., W. Baumgartner, H. J. Gruber, K. Schilcher, and H. Schindler. 1996. Detection and localization of individual antibody-antigen recognition events by atomic force microscopy. *Proc. Natl. Acad. Sci. USA.* 93:3477–3481.

27. Olave, I. A., S. L. Reck-Peterson, and G. R. Crabtree. 2002. Nuclear actin and actin-related proteins in chromatin remodeling. *Annu. Rev. Biochem.* 71:755–781.

28. Smith, C. L., R. Horowitz-Scherer, J. F. Flanagan, C. L. Woodcock, and C. L. Peterson. 2003. Structural analysis of the yeast SWI/SNF chromatin remodeling complex. *Nat. Struct. Biol.* 10:141–145.

29. Leschziner, A. E., B. Lemon, R. Tjian, and E. Nogales. 2005. Structural studies of the human PBAF chromatin-remodeling complex. *Structure (Camb).* 13:267–275.

30. Narlikar, G. J., M. L. Phelan, and R. E. Kingston. 2001. Generation and interconversion of multiple distinct nucleosomal states as a mechanism for catalyzing chromatin fluidity. *Mol. Cell.* 8:1219–1230.

31. Vicent, G. P., A. S. Nacht, C. L. Smith, C. L. Peterson, S. Dimitrov, and M. Beato. 2004. DNA instructed displacement of histones H2A and H2B at an inducible promoter. *Mol. Cell.* 16:439–452.

32. Flaus, A., and T. Owen-Hughes. 2001. Mechanisms for ATP-dependent chromatin remodelling. *Curr. Opin. Genet. Dev.* 11:148–154.

33. Mondal, N., and J. D. Parvin. 2001. DNA topoisomerase IIalpha is required for RNA polymerase II transcription on chromatin templates. *Nature.* 413:435–438.

34. Zimmerman, S. B., and A. P. Minton. 1993. Macromolecular crowding: biochemical, biophysical, and physiological consequences. *Annu. Rev. Biophys. Biomol. Struct.* 22:27–65.